Locating high-impedance faults in DC microgrid clusters using support vector machines

Applied Energy 308 (2022) 118338

Contents lists available at ScienceDirect

Applied Energy

journal homepage: www.elsevier.com/locate/apenergy

Locating high-impedance faults in DC microgrid clusters using support vector machines

Navid Bayati [a,*], Ebrahim Balouji [b], Hamid Reza Baghaee [c], Amin Hajizadeh [d], Mohsen Soltani [d], Zhengyu Lin [e], Mehdi Savaghebi [a]

[a] Electrical Engineering Section, Department of Mechanical and Electrical Engineering, University of Southern Denmark, DK-5230 Odense, Denmark
[b] Department of Signals and Systems, Chalmers University of Technology, Gothenburg, Sweden
[c] Department of Electrical Engineering, Amirkabir University of Technology, Iran
[d] AAU Energy, Aalborg University, Denmark
[e] Wolfson School of Mechanical, Electrical and Manufacturing Engineering, Loughborough University, UK

HIGHLIGHTS

- This article presents a fault location scheme based on support vector machines that works equally well for a DC Microgrid cluster.
- The proposed method is also without any communication link in methodology or implementation in the system.
- The scheme proved to work during different fault resistances from low to high resistance values within an appropriate accuracy.
- This eliminates require of communication link, and moreover, it also distinguishes the high impedance faults and noises.
- The fault location scheme is tested by experimentation setups, and the effectiveness of the proposed method is validated during different scenarios.

ARTICLE INFO

Keywords:
DC Microgrid
SVM
Fault
Clusters

ABSTRACT

With the increasing number of DC microgrids, DC microgrid clusters are emerging as a cost-effective solution. Therefore, due to the possible long distances between DC microgrids, once a fault occurs and is cleared, it should be located. Especially, locating high impedance faults (HIFs) is challenging. With communication-free fault locating methods, implementation costs can be reduced, and noise and delay of communication can be eliminated. In this paper, a novel localized fault location method using support vector machines (SVMs) is proposed for DC microgrid clusters. The purpose of this study is to facilitate the post fault conditions by locating the accurate place of the faults, even the challenging HIFs, by using the local measurements at one end of each line. The proposed scheme applies the faults, and fault features generated experimentally to the SVM, which is trained in Python for determining the fault location. The experimental test results prove that the proposed scheme is immune against disturbances, such as noise and bad calibration, and can efficiently and reliably estimate the location and resistance of faults with high accuracy.

1. Introduction

DC microgrid is a new concept in electric power systems and provides many advantages over traditional AC networks. Many low-carbon power sources such as PVs, FCs, and batteries are all DC. Thus, operating them in a DC system requires fewer conversion stages [1]. Moreover, DC cables can deliver more power through a cable than AC systems [2]. Also, the DC power cable does not suffer from the skin effect [3,4]; therefore, the power losses of the DC transmission are lower than the AC system with the same cables. However, a single DC microgrid has limited capacity and weak anti-disturbance ability. As a solution, DC microgrids can be connected to make a DC microgrid cluster and provide better performance than independent DC microgrid [5]. Clustering DC microgrids gains economic benefits during the grid-connected mode and mitigate power outage in blackout situations by maintaining the supply of critical loads.

Despite the benefits of the DC microgrid clusters, the protection of these systems is still a challenging task. These challenges are due to the lack of mature DC system protection standards, lack of zero-crossing

* Corresponding author.
E-mail address: navib@sdu.dk (N. Bayati).

https://doi.org/10.1016/j.apenergy.2021.118338
Received 29 July 2021; Received in revised form 20 October 2021; Accepted 2 November 2021
Available online 9 December 2021

Nomenclature

AC	Alternating current,
PV	Photovoltaic,
FC	Fuel cell,
CB	Circuit breaker,
HIF	High impedance fault,
SVM	Support vector machine,
ML	Machine learning,
WT	Wind turbine,
I_0	Initial current,
V_0	Initial voltage,
R	Sum of fault resistance and cable resistance from terminal to the fault point,
L	Cable's inductance from the terminal to the faulty point,
C	Capacitor of the converter,
s	Laplace operator,
R_m	Resistance of cable for each meter,
L_m	Inductance of cable for each meter,
d	Distance between terminal and faulty point,
R_f	Fault resistance,
w	Weight factor,
x	Samples,
b	Bias,
z	Distance to support vector,

points, and less research on DC CBs [6]. Moreover, during the fault, each power source unit injects a fault current into the faulty point, which results in a large and high-rise fault current, and it causes severe damages to the DC microgrid cluster components. Consequently, locating the accurate faulty place in DC microgrid clusters with high penetration of underground cables is an important challenge.

1.1. Related works

HIFs generally occur in low-voltage systems. During the HIFs, the changes in current are small. Therefore, the detection of this type of fault is challenging. Also, the accuracy of the majority of fault location methods [2] is highly dependent on the value of fault resistance. Thus, they cannot estimate the fault location by a high accuracy during HIFs. This causes difficulties in the maintenance and restoration of DC microgrid clusters after clearing the fault.

The DC fault location strategies can be divided into offline and online methods [7]. The online fault location schemes use the current and voltage measured values within the fault time and tripping of CBs to calculate the fault location. In [8], an analytical online fault locating approach has been proposed, based on the ratio of the DC line voltage to a reference value. An iterative operation has also been used to improve the fault location estimation accuracy, but it resulted in extending the tripping time of CBs. In [9], the authors have suggested a method based on the boundary-inductance-based and least-square methods to estimate the fault location in DC microgrids. However, this method has low accuracy for HIFs, and is only applicable to radial DC systems. Other online fault location strategies, such as distributed current sensing technology [10] and traveling wave-based methods [11], have been developed recently. Although these methods can locate the fault quickly, the low accuracy can lead to the false isolation of the faulty segment and possibly instability of the whole DC microgrid. Also, these methods require fault location devices at both line ends and communication links between the protection devices, which increases the cost and error rate. An online fault location scheme has been presented in [12], by utilization of the traveling-wave approach for locating the fault. However, due to the low surge arrival time, this scheme is inaccurate for DC microgrids with small line lengths. A differential fault location scheme for DC microgrids has been suggested in [13], which requires reliable and fast communication links to send the data to the protection devices. However, the data loss, communication failure, and the high cost of differential protection limit the application of these schemes.

On the other hand, the offline fault location strategies calculate the fault location after CB's tripping by using an additional auxiliary device [14]. ML and deep-learning-based fault location methods have been proposed in [15–17]. However, since most of these methods are developed for AC systems, they still face many challenges in DC microgrids. In [18,19], the injection current-based fault location schemes have been presented. In these methods, the fault location is calculated by injecting a specific signal into the DC line segment. However, these methods require a signal injection source and additional equipment. The method proposed in [20] uses a probe and a second-order RLC discharging circuit to calculate the fault location by extracting the oscillation frequency and damping envelope of the RLC circuit. Nevertheless, this method requires communication links, and it is costly and increases the noise of measured signals. The attenuation coefficient has been considered in [21] to improve the method presented in [20] and reduce the fault location error. However, the error value in the studies mentioned above is significant, more than 10% in some works, and these methods require additional equipment, which increases the cost of the protection system. On the other hand, the fault location methods in the recent studies implemented an additional fault location module [19], such as the Pearson correlation coefficient [22]. In [23], a power probe unit has been suggested for injection of the DC signals by a converter into the cable. This method operates well, however, using additional equipment increases the cost as well as human workload.

SVM is a learning-based data classification technique, which provides the maximum marginal boundary between different classes of a given data set and determines the global optimal solution. This property is recognized as the main advantage over artificial neural network-based classification approaches. SVM is a supervised learning machine where first introduced in [24] as a powerful and efficient tool for analyzing data. SVMs are not prone to be trapped in local minima like conventional neural networks. SVM builds an optimal geometric hyperplane to separate data where the data are mapped into a high dimensional feature via a non-linear mapping. Polynomial, sigmoidal and radial basis functions are widely used kernels to create separation surfaces between various functions. Only the data patterns closest to the separation surface are used for the regression process instead of all data patterns. The use of intelligent methods in fault location schemes can increase the effectiveness of the protection systems. Recently used classifiers consist of expert systems, artificial neural networks, and SVMs [25,26]. Among them, the SVM provides accurate decisions under limited samples and has better generalization ability. Thus, it has been widely used in different applications such as turboshaft engines [27], vehicle suspension systems [28], sensor fault detection [29], and health monitoring of ships [30].

1.2. Contribution of research

To the best of the author's knowledge, the proposed scheme has the highest accuracy and lowest cost among the existing local fault location systems for DC microgrids. The differences between DC and AC, meshed and radial microgrids, and with or without communication links in protection systems lead to the following challenges which are addressed in this work:

1)AC-related features such as frequency and phase characteristics are no longer available, and thus, the authors focus on new features that

Table 1
Limitations of the existing fault location methods.

Method	Advantages	Limitations
[9]	Local and low-cost method	Low accuracy, and fault resistance, only can be implemented in radial systems.
[12]	Applicable in mesh systems, and high accuracy	Requiring communication link, and high sampling rate
[13]	Fast, and accurate	Requiring communication link, and high sampling rate, only can be implemented in radial systems, and without considering fault resistances
[14]	Local, and accurate	By increasing the fault resistance and decreasing the number of fault current peaks, the fault cannot be located
[22]	Fast, accurate, and applicable in both mesh and radial systems	Requiring a high sampling rate, and analyzing data in different windows.
[23]	Without requiring communication links and external units, therefore, it is a low-cost method	Low accuracy, and fault resistance, and only can be implemented in radial systems
Proposed scheme	Local, accurate, considering fault resistances, low sampling rate, and locate HIFs	Only applicable on DC systems, requiring training before practical implementation.

may be used for fault location in DC microgrids.

2)The communication-based schemes used in DC microgrids would require a network infrastructure, high sampling rate, and filtering equipment, which might not be feasible in a low-cost DC microgrid deployment. Detailed fault analysis is represented in Section 3.

The existing fault location methods require both ends' data, and therefore, they suffer from noise and delay. Therefore, the research works presented in [12,13] cannot locate faults by using only the measured values of one end of the line segment. Furthermore, the absence of a comprehensive and accurate fault location method for HIF cases leads to an inaccurate performance of the existing methods during these types of faults. Consequently, in this research, the available features in one end of the faulty line in DC microgrids are extracted, and the application of SVM on fault location is investigated. Through extensive simulations and experimental tests, the new features and their relationship with fault location are discovered. A novel fault location scheme is designed for DC microgrid clusters based on information from the only current sensor of one end of the faulty line.

The approach is validated with experimental and simulation studies. The obtained results manifest the significance of the proposed novel scheme as there are few studies performed on the local fault location of DC microgrid clusters. The general comparison of the proposed method and existing methods are represented in Table 1. As it can be seen, most existing techniques suffer from several limitations such as high cost, requiring communication links, low accuracy, and lack of HIF location capability. The proposed scheme tried to solve the mentioned issues to provide an accurate and low-cost fault location technique.

This paper presents a new scheme for determining the accurate fault location by using the SVM technique. To the best of the authors' knowledge, this work is the pioneer for proposing SVM as a functional classifier for locating the fault location in DC microgrid clusters considering HIFs. The main contributions of paper are summarized as follows:

1) SVM (which has been previously used for many applications in electrical power engineering [27]– [30]) is used not only for determining the fault distance but also for calculating the fault resistance. In fact, the SVM performs as a dual-functional classifier to determine both fault characteristics by using fault current magnitude and slope as the features.
2) The proposed fault location scheme is developed using SVM training with superior performance compared to available ML choices such as quadratic discriminant ML, KNN, and linear discriminant in case of the accuracy of fault distance determination.
3) The proposed technique is applied to a DC microgrid cluster as a new fault location method; to the best of the authors' knowledge, no effective protection scheme has been previously proposed for such systems.

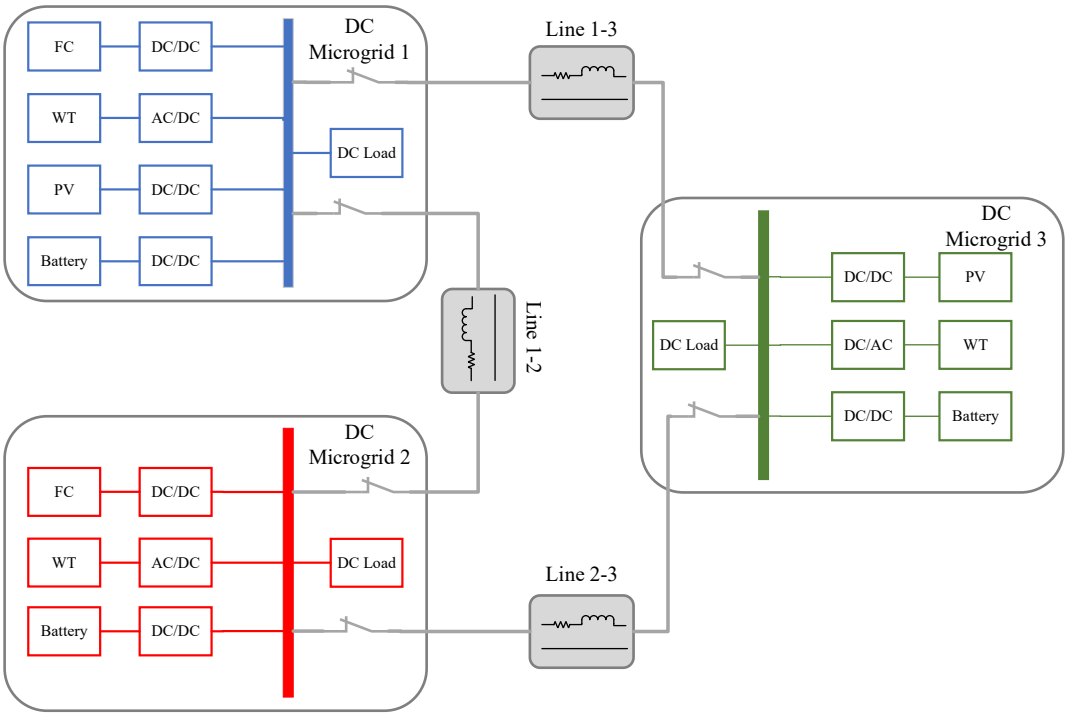

Fig. 1. Configuration of an islanded DC microgrid cluster.

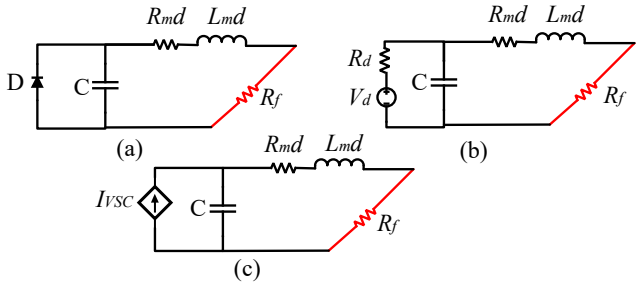

Fig. 2. The equivalent circuits of the system during (a) capacitor discharge (b) conducting freewheeling diode (c) RES current.

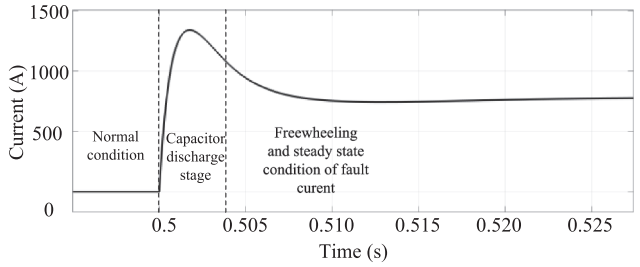

Fig. 3. Current characteristics during a fault in DC system.

4) This paper proposes the fault location scheme for low and high impedance faults up to 20 Ω. HIFs, which cause very low fault currents, have been considered limitedly in previous one-ended fault location methods for DC microgrids.
5) The proposed fault location scheme only uses the current measured at one end of the line. Therefore, it is more immune to noise compared to communication-based methods.

In this paper, a localized and offline scheme is proposed for the fault location in a DC microgrid cluster. An investigation on the possibility of using ML-based methods to develop a model to predict the location of earth fault is studied. The proposed fault location method uses the SVM to locate the accurate location of the fault in the lines of the DC microgrid cluster. In the first stage, SVM is trained in the Python programming environment by the current waveforms obtained experimentally. Then, the trained function is tested and validated in the experimental test setup. This method only requires extraction of the local current features to estimate the fault location distance to the protection device. Consequently, it reduces the cost and noise of the protection system compared to the communication-based methods. Furthermore, the proposed scheme can locate HIFs accurately, leading to improved maintenance and restoration process of the DC system. It has been tested in a hardware setup to verify its accuracy.

The remaining of this paper is organized as follows. In Section 2, the DC microgrid clusters are introduced. Section 3 elaborates on the proposed fault location method. The experimental results and discussion on the fault location function are presented in Section 4. Finally, the comparison discussions and conclusions are stated in Section 5 and 6, respectively.

2. DC microgrid cluster

Fig. 1 shows the configuration of a typical DC microgrid cluster to be studied in this paper. It includes three DC microgrids, which are interconnected to each other by DC cables. A typical DC microgrid is a combination of power converters, local loads, batteries, and RESs. In this paper, DC microgrid 1 includes FC, PV, and WT, DC microgrid 2 includes FC and WT, and DC microgrid 3 includes PV and WT. Moreover, each line is equipped with two DC CBs to isolate the lines in fault conditions to prevent fault current damage to other DC microgrids.

A high-value fault current in the DC microgrid cluster is a severe condition for power converters [31]. During faults, the fault current has two different stages: the capacitor-discharge stage and the freewheeling diode operation stage. The first stage is the discharge of the DC link capacitors immediately after the fault. The second stage starts after the capacitor's voltage reaches the minimum value of input voltage and causes the participation of RESs to the fault current through the freewheeling diodes [32]. The equivalent circuit and fault current characteristics are depicted in Figs. 2 and 3, respectively. As shown in Fig. 2 (a), during the capacitor discharge stage, the equivalent circuit is an RLC circuit, and the discharge of the capacitor injects the fault current into the faulty point. Then, as shown in Fig. 2 (b), the freewheeling diode stage starts when the voltage of the DC link capacitor reaches zero. Therefore, the voltage at the converter terminal reverses, and diodes conduct, as depicted in Fig. 2 (c). After this stage, the current is injected from the RES side to a faulty point. As illustrated in Fig. 3, during the capacitor discharge stage, the fault current is increased with a high slope to a maximum value.

2.1. Proposed protection scheme

In this section, a fault location scheme for the DC microgrid cluster is proposed. Due to the local operation of the proposed fault location function, each transmission line only requires one fault location method, which is equipped in one end of lines between DC microgrids. The main core of the fault location scheme is the SVM function, which is trained in Python and implemented into the fault location function to locate the fault location in an experimental setup. Also, since fault resistances up to 20 Ω are considered, this method can locate the HIFs with an extremely low fault current.

2.2. DC fault analysis

During the capacitor discharge stage, the line and converter can be equivalent to an RLC circuit, as shown in Fig. 2, and the magnitude of fault current during this stage can reach more than 10 times the normal current. The RLC circuit response in the frequency domain can be written as [32]

$$I(s) = \frac{\frac{V_0}{L} + I_0 s}{s^2 + \frac{R}{L}s + \frac{1}{LC}} \tag{1}$$

Thus, the time domain response of fault current based on (1) will be

$$i(t) = e^{-\alpha t}\left(-\frac{I_0\omega_0}{\omega}sin(\omega t + \beta) + \frac{V_0}{\omega L}sin(\omega t)\right) \tag{2}$$

where,

$$\begin{cases} \alpha = R/2L \\ \omega = \sqrt{1/LC - (R/2L)^2} \\ \omega_0 = \sqrt{\alpha^2 + \omega^2} \end{cases} \tag{3}$$

Then, the value of the derivative of fault current can be written as

$$\frac{di(t)}{dt} = e^{-\alpha t}\left(\frac{I_0\omega_0\alpha}{\omega}sin(\omega t - \beta) - \frac{V_0\alpha}{\omega L}sin(\omega t) - I_0\omega_0 cos(\omega t - \beta) + \frac{V_0}{L}cos(\omega t)\right) \tag{4}$$

Therefore, by substituting the (2) into (4), the derivative of fault current can be obtained by

$$\frac{di(t)}{dt} = -\alpha i(t) + \omega e^{\frac{\pi}{2\omega}\alpha} i\left(t + \frac{\pi}{2\omega}\right) \tag{5}$$

Also, the values of resistance, R, and inductance, L, can be defined by

$$\begin{cases} R = R_m d + R_f \\ L = L_m d \end{cases} \tag{6}$$

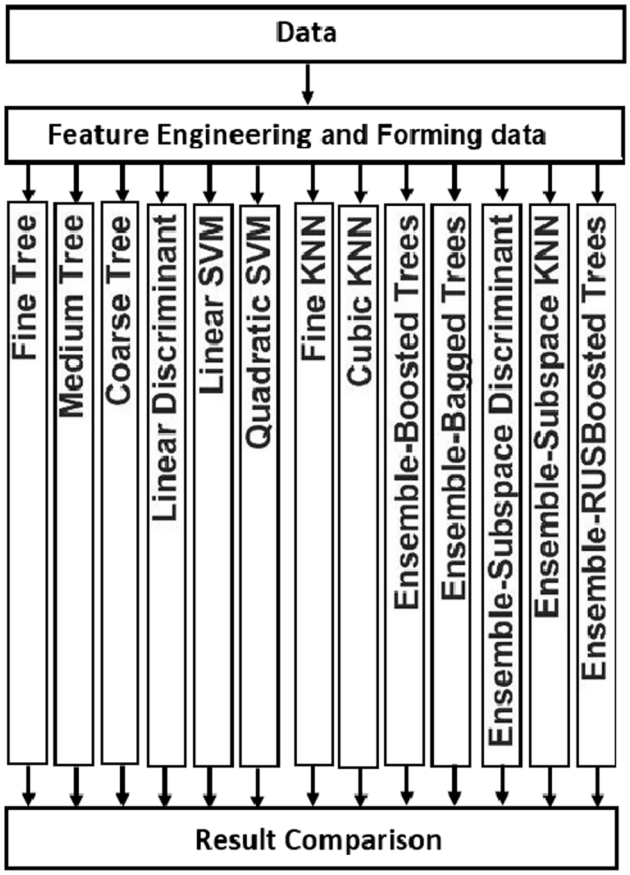

Fig. 4. The diagram of the proposed study for the prediction of fault locations.

The above equations indicate that the derivative of fault during the capacitor discharge can be determined as a function of fault current values of two different samples, fault resistance and fault location. Consequently, the proposed method, as an offline fault location method, by building a mathematical model based on sample data, can solve the unknown values.

2.3. Development of SVM-based fault location technique

In this section, the methodology of the SVM-based fault location technique will be presented. To do so, the most important features of fault current are extracted and used in the SVM method. The block diagram showing the performed studies is presented in Fig. 4. It should be noted that, in qualitative comparison, due to the advantages of SVM, such as being more effective in high dimensional spaces, cases with a greater number of dimensions than the number of samples, and cases with clear margin separation between classes, this method is selected for fault locating of DC microgrid clusters.

The available features used for developing predictor models are the maximum amplitude of fault current (I), and the derivative of the current waveform over time di/dt. To train the ML models, the training data are randomly used as a training data set (80%) and testing parts (20%).

SVM is an ML algorithm that looks to the extreme points of data sets and draws a decision boundary $w \in R^n$ among different data set classes [25]. To obtain this decision boundary, the support vectors are defined and trained based on the available features since finding the optimal boundary line, among examples. Note that the optimal boundary line is achieved using optimization tools such as quadratic, linear functions. Quadratic optimization involves minimizing or maximizing randomly defined support vector's distance from each other to bound linear equality and inequality constraints among data points. The boundary

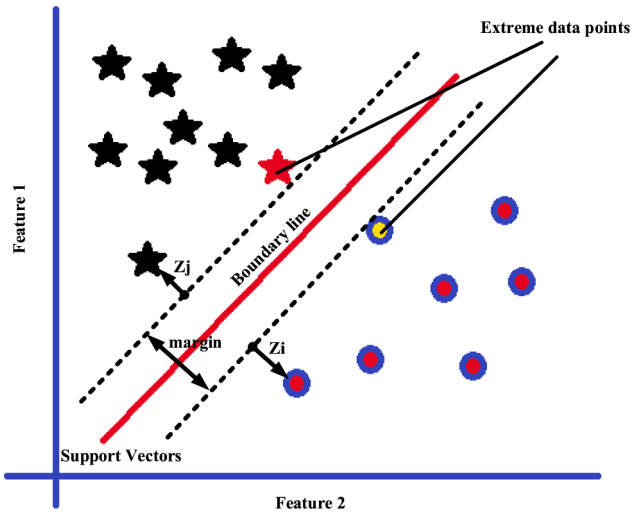

Fig. 5. Classification of data by SVM.

line that segregates classes from each other is also referred to as hyperplane because SVMs can be used in multi-dimensional data sets. A simple toy example of SVM is illustrated in Fig. 5. In Fig. 5, the formula of the boundary line can be defined as:

$$y = \langle w.x \rangle - b \tag{7}$$

In this work, the value of $\times$ is defined as the vector of [R_f, di/dt, Max($i(t)$)]. Moreover, w and b are as the vectors [2, 500, 4.5] and [2.3, 300, 4.2], respectively. Also, the margin between support vectors, shown in Fig. 5 is $2/||w||$. Thus, the optimal hyperplane can be obtained by optimization function defined as:

$$min\varphi(w,b,z) = \frac{1}{2\|w\|^2} + Q\sum_{i=1}^{m} z_i \tag{8}$$

Such that $\begin{cases} y_i(w.x_i - b) + z_i \geqslant 1 \\ z_i \geqslant 0 \ \forall i = 1, 2, 3, \ldots, m \end{cases}$

where positive constant Q is tuned to reach the optimal hyperplane, which is selected as $Q = 23$ in this work. In this work, the SVM is used to define the hyperplanes that can address faults according to extracted features. Suppose that we want to find out the location of faults according to the features of fault currents, the magnitude and derivative of fault current. Fig. 5 shows the linear hyperplane in a two-dimensional space.

To solve the fault location problem in DC microgrid clusters, the SVM technique is utilized. The main problem in using SVM is the generation and selection of features to solve the problem in the best unique way. The block diagram of the proposed methodology is presented in Fig. 6 to illustrate the inputs and output of the SVM fault location unit. Therefore, in the proposed solution, the fault location scheme relies on two features:

- The magnitude of fault current at one terminal of the line segment,
- The slope of current, di/dt, during fault at the same terminal of the line segment,

It will be presented in Section 4 that the faulty current characteristics are not unique and greatly depend on fault resistance as well as the fault distance from the fault locator terminal. It means that estimating the fault distance by only relying on fault current magnitude will not provide accurate results. To improve the accuracy of the fault location technique, the use of the slope of fault current, di/dt, is proposed in this paper. The analysis described in Section 3.1, and practical investigations in Section 4 have confirmed that the slope of fault current directly depends on the fault resistance and location. This information is used to

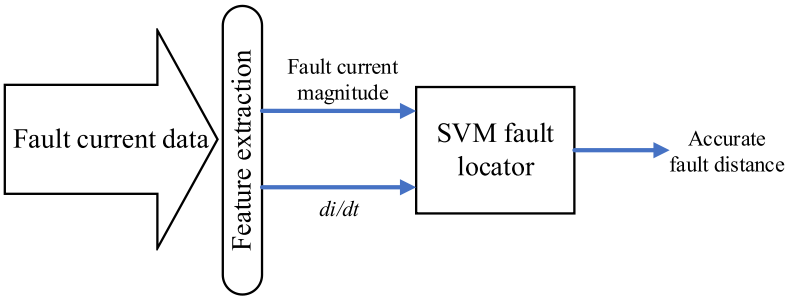

Fig. 6. Block diagram of the proposed methodology.

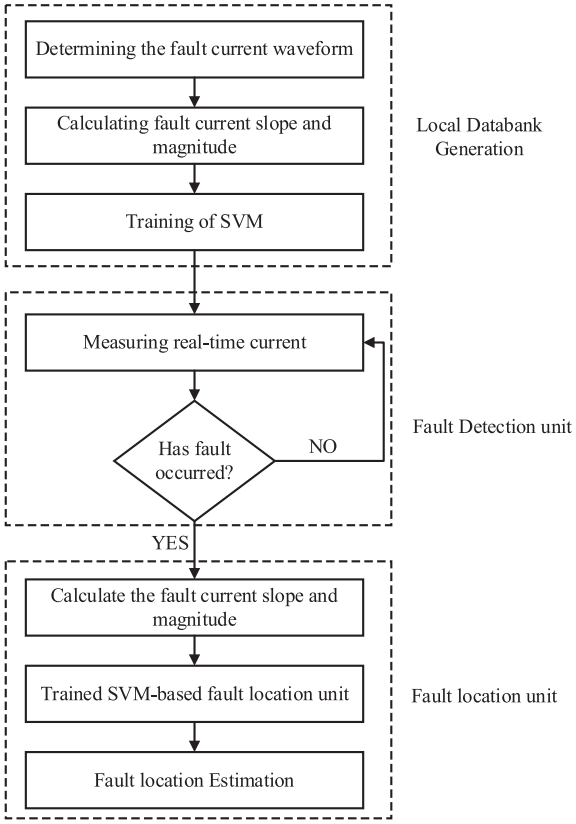

Fig. 7. Flowchart of the proposed method.

correctly locate the distance of fault. The flowchart of the proposed method is shown in Fig. 7.

3. Performance evaluation

The efficiency of the proposed fault location scheme for DC microgrid clusters has been evaluated in terms of the accuracy of the fault location against various test cases and considering HIFs. The different fault cases considered for performance analysis involve variation in fault resistance up to 20 Ω, and fault location 0–3600 m, and the connected sensors to fault location method use the sampling rate of 25 kHz. The experimental test setup is depicted in Fig. 8. The nominal voltage of the lab-scaled test setup is 24 V, and the line between DC microgrids of Fig. 1 is modelled by three resistances and inductances with values of 0.16 Ω and 10 mH, respectively, which each one is equivalent to 1200 m cable. Therefore, the R_m and L_m are 133 μΩ/meter, and 8.3 μH/meter, respectively. The detailed parameters of the experimental setup are presented in Table 2.

For training the fault location technique, 400 cases have been tested in different fault resistances and locations. The feature space model of the whole data based on *di/dt* concerning *I* and *R* is illustrated in Fig. 9 (a) and (b). As shown in Fig. 10, different ML methods, namely, quadratic discriminant ML, KNN, linear discriminant, ensemble learning, and SVM, are analyzed to find the optimum method. It is observed that the quadratic support vector machine (QSVM) [33] and fine k-nearest neighbor algorithm (KNN) [34] resulted in the highest accuracy to predict resulted in the highest accuracy for the prediction of faults location. Also, it has been found that ensemble learning presents the lowest accuracy.

Fig. 11 (a) and (b) illustrate the performance of quadratic discriminant and SVM algorithms in detail. The 1 to 4 numbers in legend representing the fault locations, and the correct (●) and incorrect (×) signs presenting the correct and wrong prediction of the model, respectively. It can be observed that the SVM method can successfully classify features from the test data set with no mistakes. However, with no proper model, such as quadratic discriminant, some of the features have not been assigned to the right class, which is illustrated with a cross sign in Fig. 11 (a).

The proposed method only requires the current measurement of one side of the line. The magnitude and derivative of the fault current are extracted for each case to design the fault location technique. Therefore, during the fault, these features are measured to locate the fault location by fault location technique. For example, for a fault at $d = 1200$ m, with $R_f = 3.2$ Ω, at $t = 8.2$ s, the fault current characteristic is shown in Fig. 12. In this case, because the $\alpha^2 < \omega_0{}^2$, as discussed in Section 3.1, the fault current is underdamped, and the value of peak is 6.27 A, and the slope value is 734 A/s. This high value of slope shows the low-rise time in this type of fault. Thus, a higher sampling rate provides more accurate results of the fault location method. On the other hand, the inequality $\alpha^2 < \omega_0{}^2$ can be rewritten as

$$4L^2C^2 < 4 - R^2C^2 \tag{9}$$

Therefore, by increasing the value of R_f, the value of $4\text{-}R^2C^2$ will be reduce, then the fault current will change to an overdamped current, since $\alpha^2 > \omega_0{}^2$.

The values of fault current features for different fault locations are presented in Table 3. As shown in Table 3, by increasing the value of fault resistance, the fault current magnitude and slope reduce. Moreover, by increasing the distance of the faulty point from the measurement unit, the measured value of the fault current magnitude and slope also decrease. The trends of fault current magnitude and *di/dt* reductions while increasing the fault resistance are shown in Figs. 13 and 14, respectively. These figures prove the small change of fault current during HIFs, which reduces the accuracy of traditional fault location methods.

Table 4 represents the results of the HIF location using the data of different fault situations. Since the interconnected line is configured by using three separate inductances, as shown in Fig. 8, the possible scenarios for fault locations are limited to four different scenarios, and the proposed method is used SVM to estimates the faulty locations in a wide range of HIF fault resistances. Since the minimum fault location and

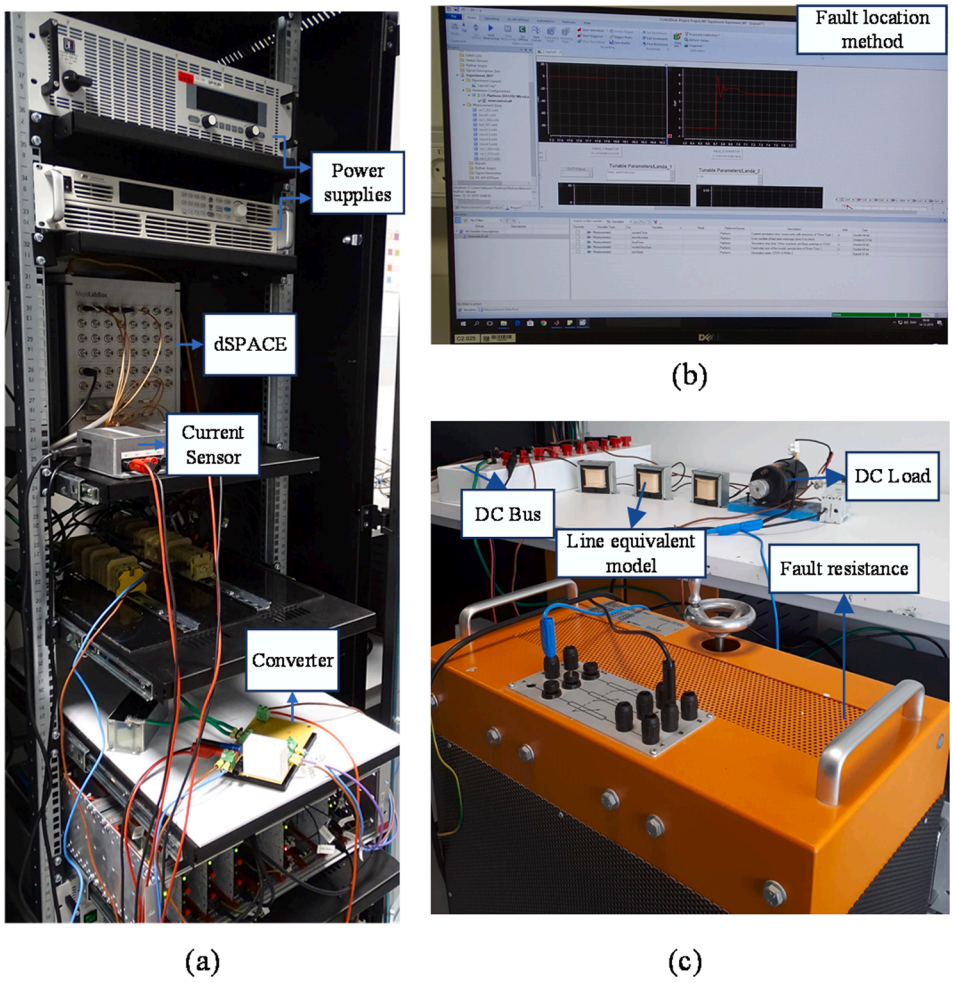

Fig. 8. Experimental setup (a) dSPACE, converter, power supplies (b) fault location technique (c) fault resistance, DC bus, DC load, and line equivalent model.

Table 2
Parameters of the hardware test setup.

Component	Parameter
Line	Resistance = 133 μΩ/m, Inductance = 8.3 μH/m
Power supply	EA-PS 390 9360, APM-SP800VDC
Sampling rate of sensors	25 kHz
Motor	DC Motor 10 W
Electronic control unit	dSPACE
Nominal voltage	24 V
Maximum R_f	20 Ω

resistance estimation accuracy is approximately 96%, based on Table 4, the performance of the proposed scheme to locate faults in DC systems is excellent. For the maximum value of fault resistance considered in this work, 20 Ω, the proposed method is not notably influenced by changing the fault resistance.

The DC sensors measure the currents during the fault with a certain value of error, and load and temperature fluctuations significantly affect the sensor accuracy [35]. Thus, the measured data are typically different from the actual data, and the fault location schemes should consider the noise impact. In this paper, the noise of measurement is considered by multiplying the measured current values by a normal, randomly generated distribution with zero mean and a standard deviation. Furthermore, to evaluate the performance of the proposed scheme during noisy input data, each measured value is multiplied by a normally distributed random number with zero mean and 1% and 2% standard deviations. The results with noisy input data are represented in

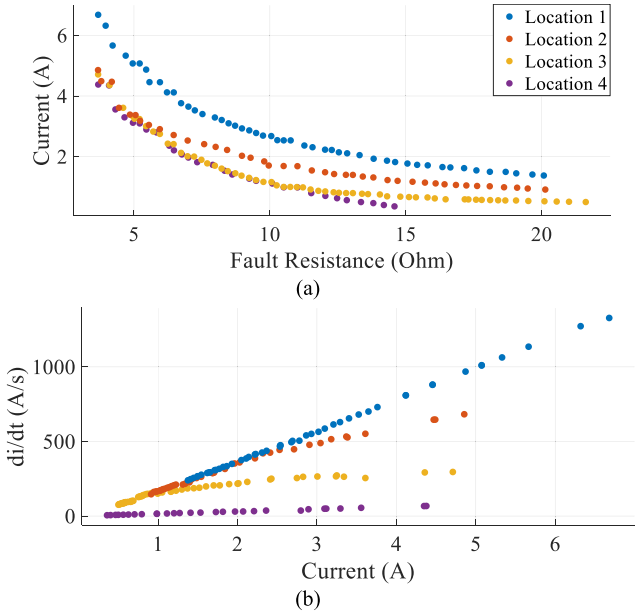

Fig. 9. Feature space model of faults according to (a) *I-di/dt*. (b) *R-I*.

2.1 ☆ Tree Last change: Fine Tree	Accuracy: 80.6% 3/3 features
2.2 ☆ Tree Last change: Medium Tree	Accuracy: 80.6% 3/3 features
2.3 ☆ Tree Last change: Coarse Tree	Accuracy: 75.0% 3/3 features
2.4 ☆ Linear Discriminant Last change: Linear Discriminant	Accuracy: 72.2% 3/3 features
2.5 ☆ Quadratic Discriminant Last change: Quadratic Discriminant	Accuracy: 97.2% 3/3 features
2.6 ☆ SVM Last change: Linear SVM	Accuracy: 94.4% 3/3 features
2.7 ☆ SVM Last change: Quadratic SVM	Accuracy: **100.0%** 3/3 features
2.12 ☆ KNN Last change: Fine KNN	Accuracy: **100.0%** 3/3 features
2.16 ☆ KNN Last change: Cubic KNN	Accuracy: 94.4% 3/3 features
2.18 ☆ Ensemble Last change: Boosted Trees	Accuracy: 33.3% 3/3 features
2.18 ☆ Ensemble Last change: Boosted Trees	Accuracy: 33.3% 3/3 features
2.19 ☆ Ensemble Last change: Bagged Trees	Accuracy: 97.2% 3/3 features
2.20 ☆ Ensemble Last change: Subspace Discriminant	Accuracy: 61.1% 3/3 features
2.21 ☆ Ensemble Last change: Subspace KNN	Accuracy: 66.7% 3/3 features
2.22 ☆ Ensemble Last change: RUSBoosted Trees	Accuracy: 94.4% 3/3 features

Fig. 10. Comparison errors of different ML methods.

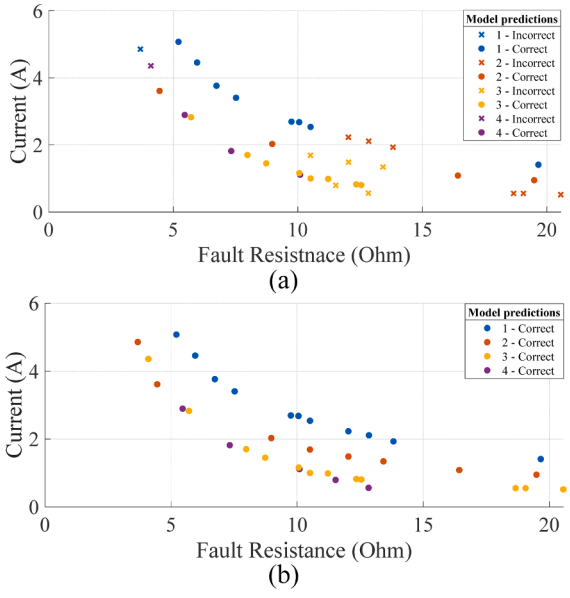

Fig. 11. Performance of (a) quadratic discriminant and (b) SVM algorithms.

Table 5 and Table 6. Moreover, the performance of the proposed method with measurement calibration error is assessed. For this aim, all measurements are considered to have 1% noise, and for considering bad calibration, the measured magnitudes are multiplied by 1.05. The results are shown in Table 7 [15].

Tables 5 and 6 show that the errors of fault location and resistance

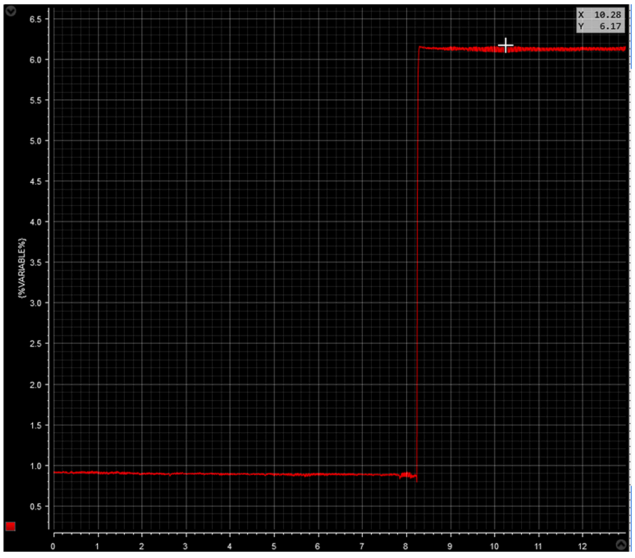

Fig. 12. Fault current performance for fault at $d = 1200$ m, with $R_f = 3.2\ \Omega$.

Table 3
Fault current features for different fault conditions.

Fault location	Fault resistance	Current Magnitude	Slope of fault current
0 m	3.683 Ω	6.68 A	1327.8 A/s
0 m	4.215 Ω	5.665 A	1135.2 A/s
1200 m	4.852 Ω	3.385 A	527.39 A/s
1200 m	5.225 Ω	3.18 A	515.20 A/s
2400 m	5.954 Ω	2.748 A	255.00 A/s
2400 m	7.214 Ω	2.001 A	217.02 A/s
2400 m	16.466 Ω	0.591 A	93.15 A/s

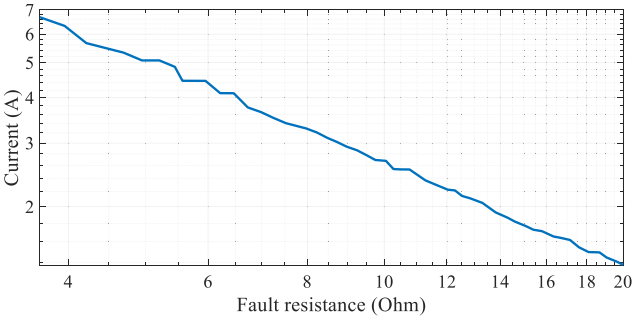

Fig. 13. Fault current magnitude trend in terms of fault resistance variation.

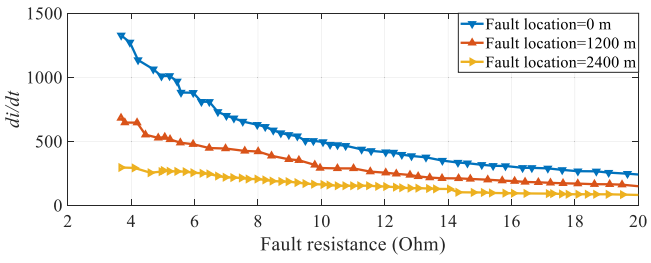

Fig. 14. Fault current slope in terms of fault resistance and fault locations.

estimation for noisy cases and noise-free situations in Table 4 are approximately the same. The average error for fault without considering noise for all fault resistance cases is 1.821 %, and it remains

Table 4
Results for fault location using proposed scheme.

Fault location (m)	Fault resistance (Ω)	*di/dt* (A/s)	Error (%)
0	6.215	809.6	1.51
1200	3.678	682.29	4.13
1200	16.847	180.10	2.36
2400	7.214	217.02	2.10
2400	18.105	86.71	1.40
3600	9.495	19.02	0.33
3600	13.807	7.87	0.92

Table 5
Fault location using proposed scheme with noise generated (0,1%).

Fault location (m)	Fault resistance (Ω)	*di/dt* (A/s)	Error (%)
0	6.215	801.77	0.73
1200	3.678	675.69	3.37
1200	16.847	178.35	4.35
2400	7.214	214.92	1.95
2400	18.105	85.87	1.24
3600	9.495	18.83	0.26
3600	13.807	7.79	0.74

Table 6
Fault location using proposed scheme with noise generated (0,2%).

Fault location (m)	Fault resistance (Ω)	*di/dt* (A/s)	Error (%)
0	6.215	806.0257	0.17
1200	3.678	679.2778	4.27
1200	16.847	179.3049	5.13
2400	7.214	216.0619	2.51
2400	18.105	86.3272	0.63
3600	9.495	18.9360	0.25
3600	13.807	7.8353	0.61

Table 7
Results for fault location using proposed scheme with noise generated (0,1%) and bad calibration in sensor.

Fault location (m)	Fault resistance (Ω)	*di/dt* (A/s)	Error (%)
0	6.215	842.0360	0.18
1200	3.678	709.6254	4.27
1200	16.847	187.3156	5.13
2400	7.214	225.7147	2.51
2400	18.105	90.1840	0.64
3600	9.495	19.7820	0.255
3600	13.807	8.1853	0.60

approximately constant during a 1% noise situation by 1.805% error and increases slightly to 1.93% for 2% noise conditions. The results of Table 7 with bad calibration show a small increase in the error of fault location estimation to 1.94%; however, it remains acceptable.

4. Discussion and comparison

In [36], a differential-based fault location strategy for calculating the distance of fault location in a PV-based DC microgrid is suggested. By estimating the unknown DC line resistance accurately by the non-iterative Moore–Penrose pseudo inverse technique, the fault distance is calculated using the measured values of two ends of each line segment, which requires communication link, current, and voltage sensors. Thus, the communication links increase the cost and noise, and also, in this strategy, the considered fault resistance is limited to 2 Ω with a maximum error of 6%. Therefore, the HIFs are not considered in this method.

The suggested schemes in [21] and [37] use additional equipment for locating faults in DC microgrids. In [21] and [38], an inductance and RLC based fault locator is installed at each end of the line, respectively. After a fault, the stored energy of the fault locator is released in the circuit to locate the fault by using the measured values of current. However, the maximum fault resistance and error of [37] are 10 Ω and 13%, respectively. Also, in [21], these maximum values are 2 Ω and 8%, respectively. Both schemes require a communication link, which increases the cost of the protection system.

In [38], the fault location of DC microgrids is calculated by solving transient equations of fault current and neural networks, respectively. In both methods, the transient measured values of current and voltage for both sides of the faulty segment are sent through a communication link to a fault location calculator function. However, the fault location during HIFs is considered in [36]. The suggested methods in [9] and [39] are designed without utilizing communication links. However, these methods cannot locate the HIFs, and the error for low-impedance faults is also high. The localized fault detection in [40] uses the *di/dt* trend of fault current to locate the fault in a radial branch of the DC Microgrid equipped with CPLs.

In this paper, a cost-effective fault location scheme for DC microgrid clusters during HIFs is proposed, which can be implemented using only local measurement units. In the proposed method, the fault location technique is installed at one end of the line segment. Therefore, this method does not require communication links, and it eliminates the noise and reduces the cost of the protection system. Moreover, because this method only needs the current sensor thus, it decreases the cost of implementation of the proposed fault location technique even more. The maximum fault resistance and error in this paper are 20 Ω, and 5 %, respectively, which shows a very good performance. The summary of the comparison between the proposed method and existing methods is indicated in Table 8.

Table 8
Comparison of the proposed scheme with other existing DC fault location methods.

Method	Cost	Maximum Error	Maximum fault resistance	HIF function	Communication links	Topology	Noise	Current sensor	Voltage sensor
[9]	Moderate	17%	2 mΩ	No	No	Radial	Not Considered	Yes	Yes
[21]	Extremely high	8%	2 Ω	No	Yes	Ring	Considered	Yes	No
[36]	Moderate	6%	2 Ω	No	Yes	Radial	Considered	Yes	Yes
[37]	Extremely high	13%	10 Ω	Yes	Yes	Ring	Considered	Yes	No
[38]	Extremely High	2%	2.4 Ω	No	Yes	Ring	Considered	Yes	Yes
[39]	Moderate	4.7%	1 Ω	No	No	Ring	Considered	Yes	Yes
[40]	Low	4%	20 Ω	Yes	No	Radial	Considered	Yes	No
Proposed Method	Low	5%	20 Ω	Yes	No	Ring	Considered	Yes	No

5. Conclusion

An SVM-based fault location method for DC microgrid clusters is proposed in this paper to overcome the limitations of the existing schemes, such as a high error for HIFs, high cost, and vulnerability to communication noises. A fault location technique is designed and connected at one end of each line of a DC line segment to eliminate the need for the communication link. The proposed scheme only requires local current samples to calculate the accurate location of the faulty point. The fault location strategy is implemented using fault current magnitude and slope as extracted features of the measured current at the fault location device side. The results prove that significant features can be extracted by the proposed method to allow fault location from a single current signal measurement. The feasibility of the proposed scheme is verified by a lab-scaled DC microgrid cluster and compared with some existing methods. The comparisons show that the proposed fault location scheme is more accurate than other methods, especially for HIFs. The proposed communication-free fault location scheme has improved different protection aspects such as cost, error, accuracy, especially for challenging cases of locating HIFs. In the future, the performance of the proposed can be enhanced by extensive analysis of the other available features of the current and voltage waveforms to investigate the feasibility of this approach for different practical applications. Moreover, the combination between different signal processing and deep-learning tools will be the basis for developing fault location units based on the proposed approach, considering all real-world limitations and challenges.

CRediT authorship contribution statement

Navid Bayati: Methodology, Writing – original draft. **Ebrahim Balouji:** Methodology. **Hamid Reza Baghaee:** . **Amin Hajizadeh:** Supervision. **Mohsen Soltani:** Supervision. **Zhengyu Lin:** Writing – review & editing. **Mehdi Savaghebi:** Writing – review & editing.

Declaration of Competing Interest

The authors declare that they have no known competing financial interests or personal relationships that could have appeared to influence the work reported in this paper.

References

[1] Liu J, Zhang W, Rizzoni G. Robust Stability Analysis of DC Microgrids With Constant Power Loads. IEEE Trans Power Sys 2018;33(1):851–60.

[2] Bayati N, Hajizadeh A, Soltani M. Protection in DC microgrids: a comparative review. IET Smart Grid 2018;1(3):66–75.

[3] B. Severino and K. Strunz, "Enhancing Transient Stability of DC microgrid by Enlarging the Region of Attraction Through Nonlinear Polynomial Droop Control," in *IEEE Trans. on Circuits and Systems I: Regular Papers*, vol. 66, no. 11, pp. 4388-4401, Nov. 2019.

[4] Sahoo SK, Sinha AK, Kishore NK. Control Techniques in AC, DC, and Hybrid AC–DC microgrid: A Review. IEEE J Emerging Selected Topics Power Electron 2018;6(2):738–59.

[5] Zhou X, Zhou L, Chen Y, Guerrero JM, Luo A, Wu W, et al. A microgrid cluster structure and its autonomous coordination control strategy. Int J Electr Power Energy Syst 2018;100:69–80.

[6] Bayati N, Baghaee HR, Hajizadeh A, Soltani M. A fuse saving scheme for dc microgrids with high penetration of renewable energy resources. IEEE Access 2020;8:137407–17.

[7] Bayati N, Baghaee HR, Hajizadeh A, Soltani M, Lin Z. Mathematical morphology-based local fault detection in DC Microgrid clusters. Electr Power Syst Res 2021;192:106981. https://doi.org/10.1016/j.epsr.2020.106981.

[8] Yang J, Fletcher JE, O'Reilly J. Short-circuit and ground fault analyses and location in VSC-based DC network cables. IEEE Trans Ind Electron 2012;59(10):3827–37.

[9] Feng X, Qi L, Pan J. A novel location method and algorithm for DC distribution protection. IEEE Trans Ind Appl 2017;53(3):1834–40.

[10] D. Tzelepis, G. Fusiek, A. Dýsko, P. Niewczas, C. Booth, and X. Dong, "Novel fault location in MTDC grids with non-homogeneous transmission lines utilizing distributed current sensing technology," *IEEE Trans. Smart Grid*, vol. 9, no. 5, pp. 5432–5443, Sep. 2018.

[11] Azizi S, Sanaye-Pasand M, Abedini M, Hasani A. A Traveling-Wave-Based Methodology for Wide-Area Fault Location in Multiterminal DC Systems. IEEE Trans. on Power Delivery 2014;29(6):2552–60.

[12] Nanayakkara OMKK, Rajapakse DA, Wachal R. Traveling-wavebased line fault location in star-connected multiterminal HVDC systems. IEEE Trans. Power Deliv. 2012;27(4):2286–94.

[13] Fletcher, Steven DA,et al."High-speed differential protection for smart DC distribution systems." IEEE Transactions on Smart Grid, vol. 5, no. 5, pp. 2610-2617, 2014.

[14] Bayati N, Baghaee HR, Hajizadeh A, Soltani M, Lin Z, Savaghebi M. Local Fault Location in Meshed DC Microgrids Based On Parameter Estimation Technique. IEEE Syst J 2021.

[15] Majidi M, Etezadi-Amoli M, Sami Fadali M. A Novel Method for Single and Simultaneous Fault Location in Distribution Networks. IEEE Trans. on Power Systems 2015;30(6):3368–76.

[16] Shafiullah Md, Abido MA, Al-Hamouz Z. Wavelet-based extreme learning machine for distribution grid fault location. IET Gener Transm Distrib 2017;11(17):4256–63.

[17] Akmaz D, Mamiş MS, Arkan M, Tağluk ME. Transmission line fault location using traveling wave frequencies and extreme learning machine. Electr Power Syst Res 2018;155:1–7.

[18] Zhengyou H, Jun Z, Wei-hua L, Xiangning L. Improved fault location system for railway distribution system using superimposed signal. IEEE Trans. Power Del. 2010;25(3):1899–911.

[19] Y. Bai,W. Cong, J. Li, L. Ding, Q. Lu, and N. Yang, "Single phase to earth fault location method in distribution network based on signal Injection principle," in Proc. 4th Int. Conf. Elect. Utility Deregulation Restruct. *Power Technol.*, Jul. 2011, pp. 204–208.

[20] Park JD, et al. DC ring-busmicrogrid fault protection and identification of fault location. IEEE Trans. Power Del. 2013;28(4):2574–84.

[21] Mohanty R, Balaji USM, Pradhan AK. An accurate noniterative fault-location technique for low-voltage DC microgrid. IEEE Trans. Power Del. 2016;31(2):475–81.

[22] Kong L, Nian H. Fault detection and location method for mesh-type DC microgrid using pearson correlation coefficient. IEEE Trans Power Delivery 2021;36(3):1428–39.

[23] Christopher E, Sumner M, Thomas DWP, Wang X, de Wildt F. Fault location in a zonal DC marine power system using active impedance estimation. IEEE Trans. Appl. Ind. 2013;49(2):860–5.

[24] Boser, B.E.; Guyon, I.M.; Vapnik, V.N. A training algorithm for optimal margin classifiers. In Proceedings of the fifth annual workshop on Computational learning theory (COLT), Pittsburgh, PA, USA, 27–29 July 1992.

[25] Yan X, Jia M. A novel optimized SVM classification algorithm with multi-domain feature and its application to fault diagnosis of rolling bearing. Neurocomputing. 2018;3(313):47–64.

[26] S. E. Pandarakone, Y. Mizuno and H. Nakamura, "Distinct Fault Analysis of Induction Motor Bearing Using Frequency Spectrum Determination and Support Vector Machine," in *IEEE Trans. on Industry Applications*, vol. 53, no. 3, pp. 3049-3056, May-June 2017.

[27] Zhao Y-P, Huang G, Hu Q-K, Li B. An improved weighted one class support vector machine for turboshaft engine fault detection. Eng Appl Artif Intell 2020;94:103796. https://doi.org/10.1016/j.engappai.2020.103796.

[28] Jeong K, Choi SB, Choi H. Sensor Fault Detection and Isolation Using a Support Vector Machine for Vehicle Suspension Systems. IEEE Trans. on Vehicular Technology 2020;69(4):3852–63.

[29] Zidi S, Moulahi T, Alaya B. Fault Detection in Wireless Sensor Networks Through SVM Classifier. IEEE Sensors J. 2018;18(1):340–7.

[30] Zhou J, Yang Y, Ding SX, Zi Y, Wei M. A Fault Detection and Health Monitoring Scheme for Ship Propulsion Systems Using SVM Technique. IEEE Access 2018;6:16207–15.

[31] Fletcher SDA, Norman PJ, Galloway SJ, Burt GM. Determination of protection system requirements for DC unmanned aerial vehicle electrical power networks for enhanced capability and survivability. IET Elect. Syst. Transp. 2011;1(4):137–47.

[32] Mohanty R, Pradhan AK. Protection of Smart DC microgrid With Ring Configuration Using Parameter Estimation Approach. IEEE Trans. on Smart Grid 2018;9(6):6328–37.

[33] Hong Dug Hun, Hwang Changha. Interval regression analysis using quadratic loss support vector machine. IEEE Trans Fuzzy Systems 2005;13(2):229–37.

[34] Madeti SR, Singh SN. Modeling of PV system based on experimental data for fault detection using kNN method. Sol Energy 2018;173:139–51.

[35] M. Etezadi-Amoli, M. Ghofrani, and A. Arabali, "Performance of advanced meters: Effect of different temperature and loading conditions on the meters accuracy," in Proc. *IEEE PES Transmission and Distribution*, Apr. 14–17, 2014, pp. 1–5.

[36] Dhar S, Patnaik RK, Dash PK. Fault Detection and Location of Photovoltaic Based DC microgrid Using Differential Protection Strategy. IEEE Trans. Smart Grid 2018;9(5):4303–12.

[37] Yang Y, Huang C, Xu Q. A Fault Location Method Suitable for Low-Voltage DC Line. IEEE Trans Power Delivery 2020;35(1):194–204.

[38] Sharanya M, Devi MM, Geethanjali M. "Fault Detection and Location in DC microgrid". In2018 *National Power Engineering Conference (NPEC)* 2018 Mar 9 (pp. 1-7). IEEE.

[39] D. Wang, V. Psaras, A. A. S. Emhemed and G. M. Burt, "A Novel Fault Let-through Energy based Fault Location for LVDC Distribution Networks," *in IEEE Trans. on Power Delivery*, Early access.

[40] Bayati N, Baghaee HR, Hajizadeh A, Soltani M. Localized Protection of Radial DC Microgrids With High Penetration of Constant Power Loads. IEEE Syst J 2021;15 (3):4145–56.